

Use of Dual-Wavelength Radar for Snow Parameter Estimates

LIANG LIAO

Goddard Earth Sciences and Technology/Caelum, NASA GSFC, Greenbelt, Maryland

ROBERT MENEGHINI

NASA GSFC, Greenbelt, Maryland

TOSHIO IGUCHI

Communications Research Laboratory, Tokyo, Japan

ANDREW DETWILER

South Dakota School of Mines and Technology, Rapid City, South Dakota

(Manuscript received 4 April 2004, in final form 28 April 2005)

ABSTRACT

Use of dual-wavelength radar, with properly chosen wavelengths, will significantly lessen the ambiguities in the retrieval of microphysical properties of hydrometeors. In this paper, a dual-wavelength algorithm is described to estimate the characteristic parameters of the snow size distributions. An analysis of the computational results, made at X and Ka bands (T-39 airborne radar) and at S and X bands (CP-2 ground-based radar), indicates that valid estimates of the median volume diameter of snow particles, D_0 , should be possible if one of the two wavelengths of the radar operates in the non-Rayleigh scattering region. However, the accuracy may be affected to some extent if the shape factors of the gamma distribution used for describing the particle distribution are chosen far from the true values or if cloud water attenuation is significant. To examine the validity and accuracy of the dual-wavelength radar algorithms, the algorithms are applied to the data taken from the Convective and Precipitation-Electrification Experiment (CaPE) in 1991, in which the dual-wavelength airborne radar was coordinated with in situ aircraft particle observations and ground-based radar measurements. Having carefully coregistered the data obtained from the different platforms, the airborne radar-derived size distributions are then compared with the in situ measurements and ground-based radar. Good agreement is found for these comparisons despite the uncertainties resulting from mismatches of the sample volumes among the different sensors as well as spatial and temporal offsets.

1. Introduction

Radar has been considered as an effective tool for remotely measuring different types of precipitation. Directly relating a radar measurable, such as the radar reflectivity factor Z to the precipitation rate R , is widely used to monitor and estimate the development of a variety of storms. Sekhon and Srivastava (1970) carefully examined the measured snow size distributions reported by Imai et al. (1955), Magono (1957), and

Ohtake (1968), and proposed equations that connect the radar reflectivity to the snow rate in the form of melted water, the median volume diameter, and the liquid water content. Their approach, among others (e.g., Smith 1984; Loffler-Mang and Blahak 2001), uses a single wavelength much larger than the particle sizes so that Rayleigh scattering is appropriate for their analysis. However, in view of the complexity of snow in nature, a single wavelength radar measurement is unable to account fully for the variability arising from different meteorological conditions. As such, it is not surprising to see the existence of many Z - R relations reported in the literatures (see Gunn and Marshall 1958; Carlson and Marshall 1972; Smith 1984; Boucher and Wieler 1985; Matrosov 1992).

Corresponding author address: Dr. Liang Liao, Goddard Earth Science Technology/Caelum Research Corp., Code 614.6, NASA Goddard Space Flight Center, Greenbelt, MD 20771.
E-mail: lliao@priam.gsfc.nasa.gov

Dual-wavelength radar techniques have shown promise in accurately estimating characteristics of the size distribution when one or both wavelengths operate in the non-Rayleigh region (Matrosov 1992, 1998; Meneghini et al. 1992, 1997; Meneghini and Kumagai 1994; Liao et al. 1997; Vivekanandan et al. 2001; Mardiana et al. 2004). A spaceborne radar operating at Ku and Ka bands has been proposed as one of the core instruments for the Global Precipitation Measurements (GPM; Iguchi et al. 2002) and will serve as a calibrator for other instruments aboard the GPM satellite in mapping precipitation globally. With use of dual-wavelength radar, the ambiguities are significantly lessened for the retrieval of the microphysical properties of hydrometeors in comparison with single wavelength radars such as the Tropical Rainfall Measuring Mission (TRMM) precipitation radar (PR; Simpson et al. 1996). In this paper we begin with a discussion of a dual-wavelength algorithm by which the snow particle size distribution can be inferred. In an effort to examine its validity and accuracy, two separate cases from the Convective and Precipitation-Electrification Experiment (CaPE) in 1991 are studied. The algorithm is applied to measurements taken by a dual-wavelength (X and Ka bands) airborne radar. The retrieved results of the snow particle size distributions are then compared with those from in situ aircraft measurements and the National Center for Atmospheric Research (NCAR) CP-2 S- and X-band ground-based radars that were coordinated with the airborne radar measurements. Good agreement is found for these comparisons despite spatial and temporal offsets as well as the uncertainties resulting from mismatches of the sample volumes among the different sensors.

2. Dual-wavelength algorithm

The effective radar reflectivity factor of the hydrometeors at wavelength λ is given as

$$Z_e = \frac{\lambda^4}{\pi^5 |K_w|^2} \int_0^\infty N(D) \sigma_b(D, \lambda) dD, \quad (1)$$

where the $N(D)$ is the particle size distribution and $\sigma_b(D, \lambda)$ the backscattering cross section. The dielectric factor, K_w , is used to designate $(m^2 - 1)/(m^2 + 2)$, where m is the complex refractive index of water. By convention, $|K_w|^2$ is taken to be 0.93 (Battan 1973). While Z_e can be converted from the radar return signals, $\sigma_b(D, \lambda)$ is directly computed by Mie theory. Finding a solution to the parameters of the $N(D)$ from (1) is an inverse problem, and the focus of this paper. A more detail description of the dual-wavelength radar algorithm for the retrieval of $N(D)$ will be discussed below.

Based on measurements and model studies (Braham 1990; Gorgucci et al. 2000, 2002; Brangi et al. 2002) the hydrometeor size distributions can be conveniently described by the gamma distribution. A form of the gamma size distribution of $N(D)$, used widely in the retrieval of the microphysical properties of hydrometeors, is expressed as

$$N(D) = N_0 D^\mu \exp\left[-(3.67 + \mu) \frac{D}{D_0}\right], \quad (2)$$

where N_0 is a parameter related to the hydrometeor number density, D the snow diameter, D_0 the median volume diameter of the snow particle, and μ the shape factor. The number concentration, N_T , can be expressed in terms of these variables by

$$N_T = N_0 \Gamma(\mu + 1) / G^{\mu+1}, \quad (3)$$

$$G = (3.67 + \mu) / D_0, \quad (4)$$

where Γ is the gamma function. The radar dual-frequency ratio (DFR) in decibels, describing the difference of the radar reflectivity at two wavelengths, is defined as

$$\text{DFR} = 10 \log(Z_u / Z_v), \quad (5)$$

where Z_u and Z_v are the radar reflectivity factors at wavelengths of λ_u and λ_v . In this paper λ_u is associated with the longer wavelength (lower frequency). The DFR is independent of the N_0 as can be inferred from (1), (2), and (5). Matrosov (1992 and 1998) was the first to recognize that for constant snow densities, the DFR and D_0 relationships are nearly independent of snow density.

Snow is a mixture of ice and air. Its effective dielectric constant, which is needed in the computation of $\sigma_b(D, \lambda)$ of (1), is solely determined by the snow density (Maxwell-Garnett 1904; Debye 1929; Bruggeman 1935; Meneghini and Liao 1996, 2000; Liao and Meneghini 2000). Thus the radar reflectivity factor is also a function of the snow density. Given a D_0 the ratio of Z_u and Z_v can be computed from (1) and (2) if μ is fixed, and subsequently DFR is determined based on (5). Figures 1 and 2 show the computational results of the DFR versus D_0 for the snow size distribution given by (2) for the T-39 airborne radar that operates at X and Ka bands. To see how the snow density affects the results of the DFR- D_0 relations, the computations are made for several snow densities ranging from 0.05 to 0.8 g cm⁻³. The results depicted in Fig. 1 are for the case where $\mu = 2$. It is clearly seen that the relations between the DFR and D_0 are almost independent of the snow density for the D_0 less than 3.5 mm. These are consistent with the findings reported by Matrosov (1992, 1998). Moreover, the DFR has one-to-one cor-

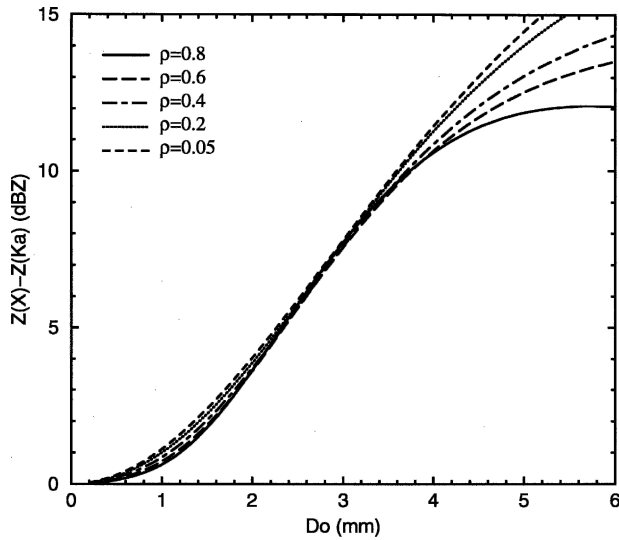


FIG. 1. DFR vs D_0 for the snow densities of 0.8, 0.6, 0.4, 0.2, and 0.05 g cm^{-3} when $\mu = 2$ for the T-39 airborne radar (X and Ka bands).

response with D_0 , which means that (5) has a unique solution for D_0 for a given DFR. The increase of DFR with D_0 can be attributed to the differences of the scattering characteristics between the approximately Rayleigh scattering at X band and non-Rayleigh scattering at Ka band. The independence of the DFR- D_0 relations on snow density is significant because the estimates of D_0 will not be affected by variations or inaccurate assumptions regarding snow density. This represents an advantage of dual-wavelength radar tech-

nique in deriving snow parameters over the single wavelength radar method in which the snow density has to be assumed.

In Fig. 2, the dependence of the DFR- D_0 relations on the parameter, μ , is shown for a fixed snow density of 0.2 g cm^{-3} as μ varies from -0.5 to 6. The results show that for a fixed DFR, D_0 increases with μ . While changes in the DFR- D_0 relations appear relatively large as μ changes from 0 to 2, the differences in the DFR- D_0 relations change more gradually as μ increases from 2 to 6. Dependence of the DFR- D_0 relations on μ may lead to an ambiguity in the estimate of D_0 if the values of μ fluctuate to a large degree. For example, a DFR of 5 dB corresponds to D_0 values of 1.99, 2.55, and 2.72 mm for μ of 0, 4, and 6, respectively.

To analyze the ground-based CP-2 radar data, the results of the DFR versus D_0 are plotted in Figs. 3 and 4 for the case of S and X bands. As the majority of snow particles are close to the Rayleigh scattering regime at S and X bands, where the radar reflectivity is independent of the wavelength, the DFR shown in Figs. 3 and 4 is typically less than 1 dBZ for D_0 up to 3 mm. The DFR- D_0 relations for the S and X bands depend on snow density (Fig. 3) and μ (Fig. 4). Because of the small dynamic range of DFR a small fluctuation in the measurement of this quantity can lead to a large error in D_0 . For example, an error of 0.2 dBZ in the DFR generally translates into a difference of about 0.5 mm of D_0 for a D_0 near 1.5 mm. This error is even greater for smaller values of D_0 . Because of this, a large number of radar samples is needed to extract the signals in order

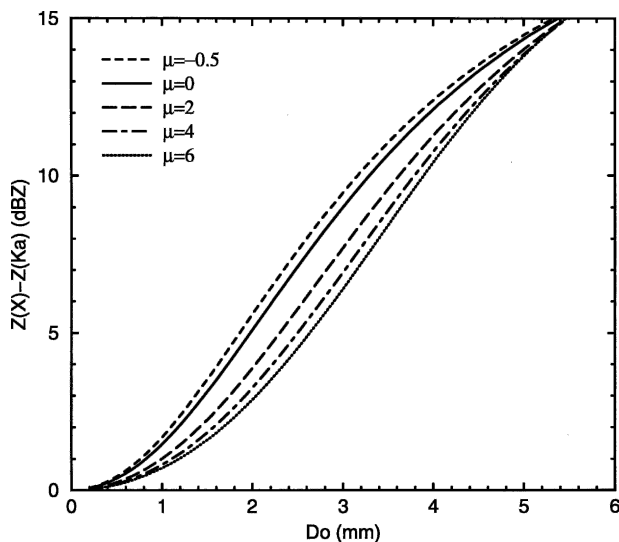


FIG. 2. DFR vs D_0 for μ of -0.5, 0, 2, 4, and 6 when the snow density is 0.2 g cm^{-3} for the T-39 airborne radar (X and Ka bands).

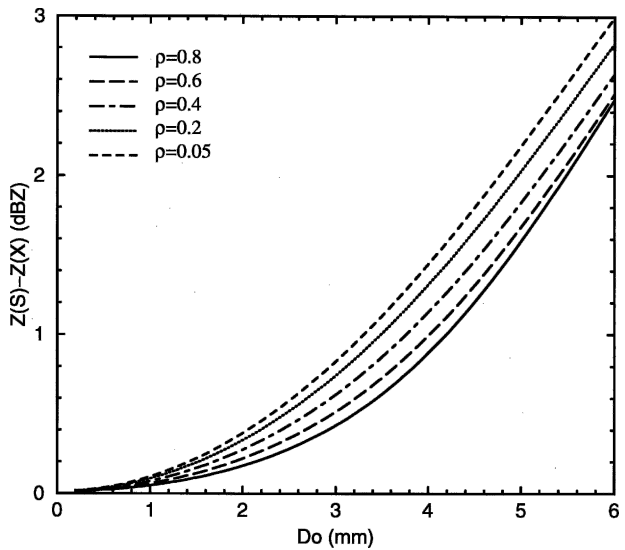


FIG. 3. DFR vs D_0 for the snow densities of 0.8, 0.6, 0.4, 0.2, and 0.05 g cm^{-3} when $\mu = 2$ for the CP-2 ground-based radar (S and X bands).

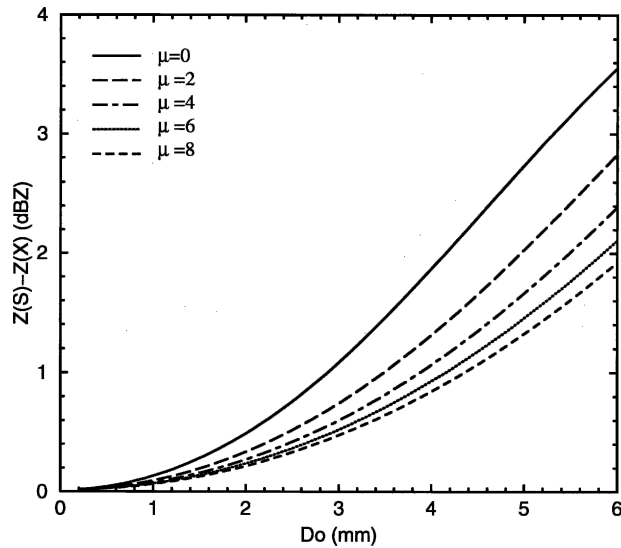


FIG. 4. DFR vs D_0 for μ of 0, 2, 4, 6, and 8 when the snow density is 0.2 g cm^{-3} for the CP-2 ground-based radar (S and X bands).

to obtain reliable retrievals of D_0 from the S- and X-band radar. Although collecting a large number of samples poses a difficulty for air/spaceborne radar systems, it is less of a problem for ground-based radars when pointed along a fixed direction or operated in a slow-scan mode. In view of the differences of the DFR– D_0 relations between the T-39 and CP-2 radars, as depicted in Figs. 1–4, wavelengths of X and Ka bands have a great advantage over a radar operating at S and X bands in terms of stability and accuracy of snow parameter estimates as long as attenuation from rain or cloud water can be neglected.

For the snow region in stratiform precipitation where the attenuation is usually negligible for airborne X- and Ka-band frequencies, D_0 can be directly estimated from the measured DFR. For ground radar, by contrast, the measured DFR in the snow region usually needs to be corrected to account for attenuation of the signal through the intervening rain. Once D_0 is known, N_T can be directly derived from the radar reflectivity at either wavelength if the snow density is either fixed or prescribed as a function of the snow particle size. As will be seen later, N_T is not only sensitive to the snow density but also to the value of μ .

We focus in the following sections on two separate case studies from CaPE that allow the comparisons of the results retrieved from the airborne dual-wavelength radar (X and Ka bands) with in situ airborne particle measurements as well as the snow size distribution parameters derived from S- and X-band ground-based radar.

3. Comparison with in situ measurements

On 19 July 1991 (1815–1845 UTC) during the CaPE conducted in the central Florida region during the period 8 July–18 August 1991, a weak convective cell was observed by an airborne radar in coordination with in situ measurements. These measurements offer an opportunity to check directly the airborne dual-wavelength algorithm for the estimates of snow parameters. The airborne radar, built by the Communication Research Laboratory of Japan, was installed on the National Aeronautics and Space Administration (NASA) T-39 aircraft. Operating at X and Ka bands, the radar viewed the precipitation at nadir with beamwidths matched at 5° . The in situ particle measurements were made using a PMS 2D-P probe mounted on the T-28 aircraft of the South Dakota School of Mines and Technology. Figure 5 illustrates the flight tracks of the T-39 and T-28 with an origin at latitude 28.35° and longitude -81.2° . The T-28 penetrated the storm twice where the start of track A occurred about 8 min before the start of the T-39 flight track leg and the start of track B about 3 min after the T-39 flight track. The offsets in space between the T-28 and T-39; that is, the horizontal distance between the T-28 aircraft and the nearest T-39 radar range gate, were generally within 5 km while the temporal offsets were within 8 min. For these flights the T-39 flew at an altitude of approximately 11 km while the T-28 flew at 5.2 km. Figure 6a displays the T-39 measurements of the X-band radar reflectivities along the flight track direction shown in Fig. 5. The origin in the plot coincides with the starting point of the T-39 flight track at time 1836:03 UTC. The white line shown

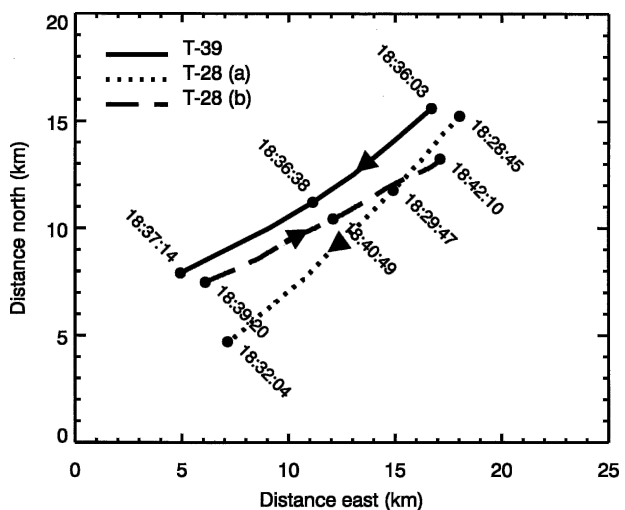


FIG. 5. Flight tracks of the T-39 and T-28 aircraft during observations of a weak convective cell with an origin at latitude 28.35° and longitude -81.2° . Time stamps are given at selected positions.

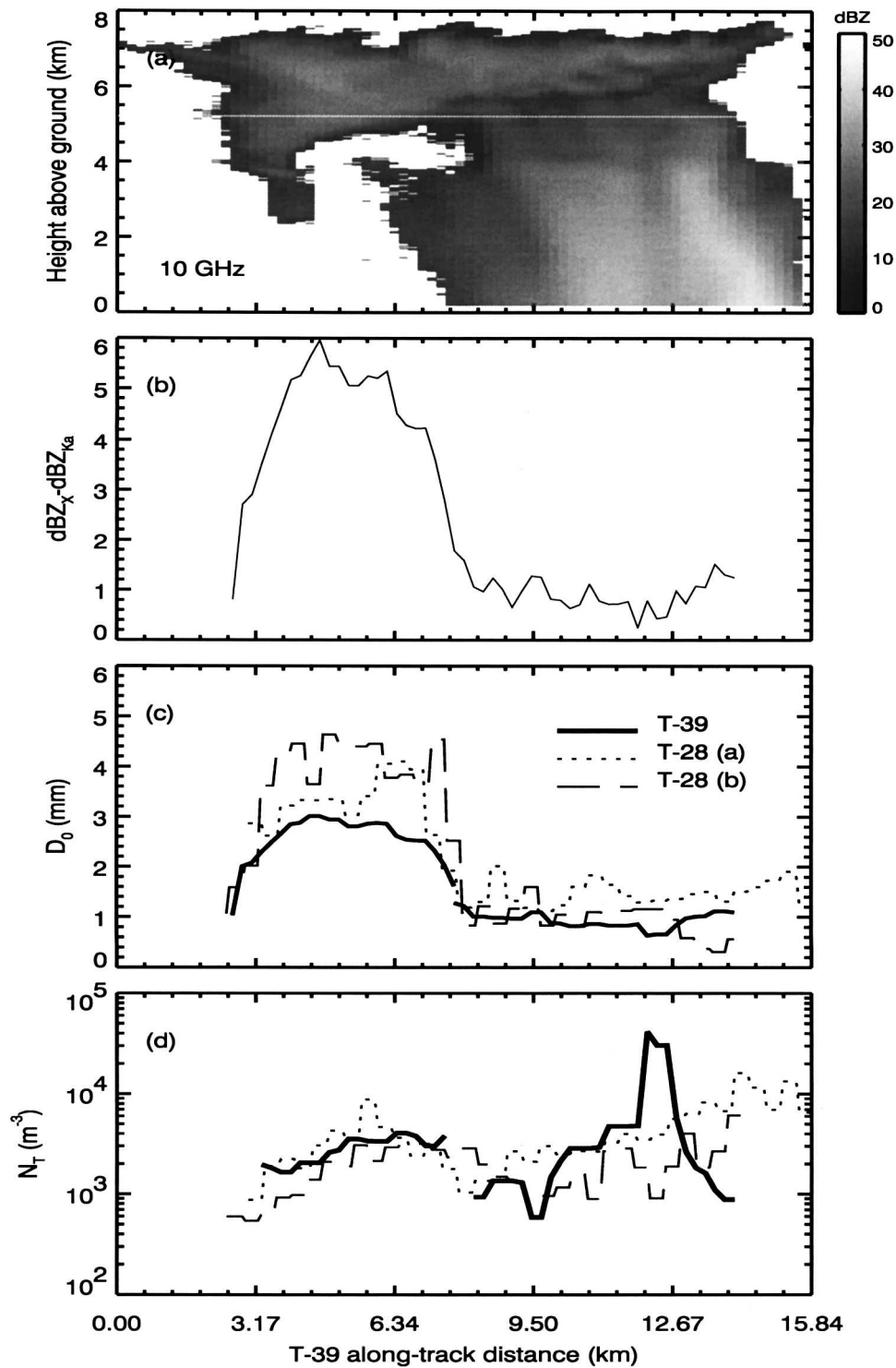


FIG. 6. Airborne radar measurements over a weak convective cell and retrievals of the size distributions in comparisons with the in situ particle measurements: (a) T-39 radar measured reflectivity at nadir along the flight track shown in Fig. 5; (b) DFR of X and Ka bands at the altitude where the T-28 flew, as indicated by the white line in (a); (c) comparisons of D_0 between the radar estimated and the 2D-P measured results; and (d) similar comparison for N_T . Note that the values of ρ and μ for the radar retrieval are 0.2 g cm^{-3} and -0.5 for aggregates and 0.7 g cm^{-3} and 1 for graupel, respectively.



FIG. 7. PMS 2D-P images taken from the T-28 aircraft of the South Dakota School of Mines and Technology. The images taken around (top) 1829:15 UTC for 4 s exclusively consist of aggregates while the measurements taken around (bottom) 1830:50 UTC are made of graupel. The vertical bars separating shadow images represent a scale of 6 mm.

in Fig. 6a indicates the T-28 flight altitude. The DFR derived from the X- and Ka-band data at 5.2 km is plotted in Fig. 6b.

Two regions can be clearly distinguished by viewing the magnitude of the DFR. Over the range from 3 to 7.5 km (region 1) the DFR attains levels as high as 6 dB, whereas for distances exceeding 7.5 km (region 2) the average DFR is close to 1 dB. Regions 1 and 2 correspond to the T-39 time segments of 1836:03–1836:38 and 1836:38–1837:14 UTC, respectively, as shown in Fig. 5. An examination of the T-28 PMS 2D-P images shows two main types of snow particles in this storm cell. For the period 1828:45–1829:47 UTC for track A and 1840:49–1842:10 UTC for track B, the particles appear to be almost exclusively aggregates. The particles viewed during the period 1829:47–1832:04 UTC for track A and 1839:20–1840:49 UTC for track B are identified as graupel by their small, nearly spherical shape. Shown in Fig. 7 are the examples of the T-28 PMS 2D-P images of the T-28 track A for the aggregates (top) measured from 1829:15–1829:19 UTC and the graupel (bottom) from 1830:50–1830:54 UTC. The snow aggregates typically have a low density ($0.05\text{--}0.2\text{ g cm}^{-3}$) while the mass densities of graupel lie between $0.4\text{--}0.8\text{ g cm}^{-3}$ (Battán 1973). Since the attenuation is negligible in dry snow at these frequencies, then if the cloud

liquid water can be neglected, the D_0 can be directly obtained from the DFR by use of the DFR– D_0 relations shown in Figs. 1 and 2. With use of D_0 and reflectivity at X band, the number concentration N_T can be computed. To compare with the in situ measurements, the airborne radar retrieval was performed using data at the height of 5.2 km where the horizontal distance between the aircraft was smallest. To overcome offsets in space and time between the T-39 and T-28, a single shift of 3 km was made for the T-28 flight track A and 2.5 km for the track B to match the T-39 observations in the aggregate and graupel regions. In this way, comparisons of the D_0 and N_T can be fairly made between the T-28 in situ measurements and the T-39 airborne radar estimates. A detailed analysis of their comparisons will be given later.

To see how the snow particle size distributions are represented by the gamma distributions, we categorize the snow particles into the aggregates and graupel based on the in situ measurements of the T-28 flight tracks shown in Fig. 5, and then parameterize the respective size distributions into the gamma distributions. Figure 8 is an example of the measurements of the size distributions of aggregates obtained from the T-28 PMS of track A. The averaged distribution of the particle size is computed based on the measured data and plot-

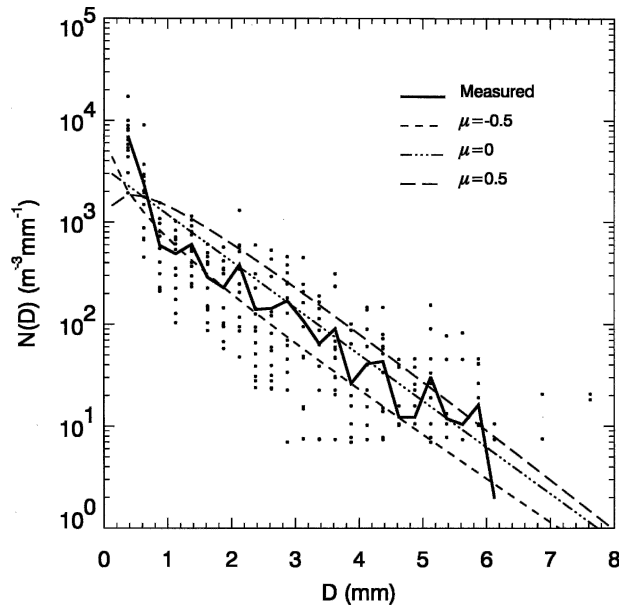


FIG. 8. Measurements of the T-28 in situ particle size distributions of snow aggregates from track A. The thick solid line represents the averaged size distribution of the measured data. The gamma size distributions are also plotted for the parameter μ of -0.5 , 0 , and 0.5 . The D_0 and N_T are, respectively, set to 3.5 mm and 3231 m^{-3} , the mean values of the median volume diameter and particle number concentration from the measurements.

ted in the thick solid line. Using the same D_0 and N_T of the measured mean distribution, the gamma size distributions are plotted in Fig. 8 for μ of -0.5 , 0 , and 0.5 . In general, the gamma distributions, as shown in Fig. 8, reasonably describe the particle size spectra. Of these parameterization curves, however, the gamma distribution with μ equal to -0.5 has the best fit for the measured data in view of their rms with respect to the measurements. Same conclusions are drawn from the analysis of the measured size spectra of aggregates from the track B; that is, the size distributions of aggregates are best represented by the gamma distributions if μ is taken to be -0.5 . For the case of graupel, it is found, from the results of parameterizations of the size spectra within the graupel regions of the T-28 tracks A and B, that μ is set to 1 for the gamma size distribution, yielding the smallest rms from the measured data. Therefore, the shape factor of the size distribution μ , is chosen to be -0.5 for aggregates and 1 for graupel for our retrievals.

Illustrated in Figs. 6c and 6d are the results of the comparisons between the T-28 measurements and the T-39 estimates. In the estimation of D_0 and N_T from the T-39 radar, particle densities of 0.2 and 0.7 g cm^{-3} are taken to characterize, respectively, the aggregates and graupel in the two regions that yield the best agree-

ments. The 2D-P measures the maximum dimension of the particle, either along the x or y axis, whichever length is larger, so that the median volume diameter, $D_{0,\text{max}}$, is expressed in terms of the maximum dimension. Therefore, to compare the estimates of particle size from the in situ and radar measurements an account must be made for the differences between $D_{0,\text{max}}$ and D_0 . For the graupel particles which are nearly spherical, the $D_{0,\text{max}}$ and D_0 are approximately the same and therefore no adjustment is made. For the aggregates it is reasonable to assume that the $D_{0,\text{max}}$ is always larger than the D_0 , which by definition, is the equivalent-volume diameter of the sphere. To account for this difference, we have scaled the D_0 estimates from the dual-wavelength radar data by a factor of 1.5 . Although the adjustment of D_0 to $D_{0,\text{max}}$ for aggregates depends on particle shape, orientation and size distribution, the scale factor of 1.5 , used in Fig. 6c, seems to work well for our comparisons. As indicated in Fig. 6, the retrievals of D_0 and N_T from the dual-wavelength radar measurements are fairly good. Some of the discrepancies between the retrieved and measured results may be attributable to offsets in the T-39 and T-28 flight tracks as well as the large differences between the sampling volumes of the radar and the PMS probe.

In Figs. 9 and 10, the inferred gamma size distributions from the T-39 for aggregates and graupel expressed as the means of the results depicted in Figs. 6c and 6d are compared with the T-28 measured mean size distributions. The procedures to obtain the averaged DSD spectra, $\overline{N(D)}$, over the aggregate and graupel regions are to sum all the derived (T-39) and measured (T-28) DSD in their respective regions and then divide by the number, n , of corresponding DSD profiles. This operation can be expressed by the following equation:

$$\overline{N(D_j)} = \frac{\sum_{i=1}^n N_i(D_j)}{n}; j = 1, \dots, m, \quad (6)$$

where D_j is the diameter of particle at the j th bin of size and m the total number of size bins. The thick lines of Figs. 9 and 10 correspond to the T-28 measurements for tracks A and B. For aggregates the scale factor of 1.5 , as mentioned earlier, is used for the radar-derived gamma distributions. Despite somewhat variations of the measured spectra, demonstrated by the differences between tracks A and B, the inferred gamma size distributions show an excellent agreement with the in situ particle measurements for both aggregates and graupel. This is an encouraging result because the snow size distribution might be accurately derived from the X- and Ka-band radar if the shape factor of the gamma distribution and the snow density are known.

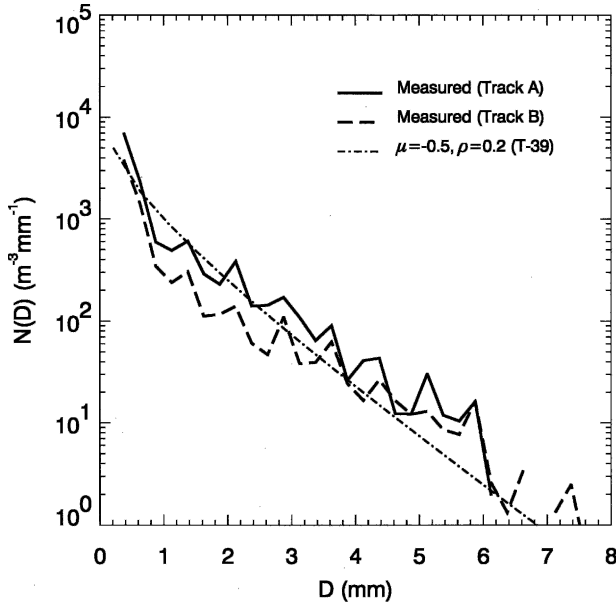


FIG. 9. Comparisons of the snow size distributions of aggregates from the T-28 in situ measurements and the T-39 radar retrievals. The average values of D_0 and N_T are, respectively, 3.5 mm and 3231 m^{-3} for the T-28 track A, 4.2 mm and 1754 m^{-3} for the T-28 track B, and 2.6 mm and 2314 m^{-3} for the T-39 radar estimates. For the T-28 data, D_0 denotes the median maximum dimension of particles; the radar-derived median volume diameter, D_0 , has been scaled by a factor of 1.5 for comparison purposes.

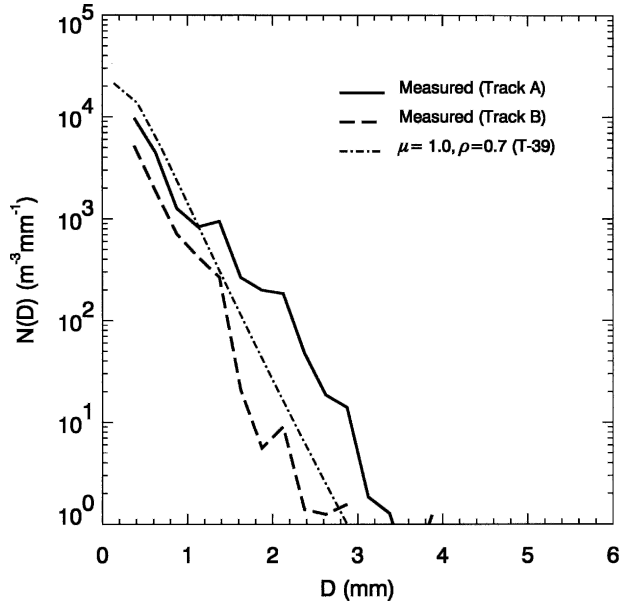


FIG. 10. Comparisons of the snow size distributions of graupel from the T-28 in situ measurements and the T-39 radar retrievals. The values of D_0 and N_T are, respectively, 1.4 mm and 4488 m^{-3} for the T-28 track A, 1.02 mm and 2125 m^{-3} for the T-28 track B, and 1.02 mm and 3433 m^{-3} for the T-39 radar estimates.

To examine how the retrieval results vary as the different parameters are used, we repeat our computations for D_0 and N_T with different values of ρ and μ . Let $\rho = (\rho_1, \rho_2)$ denote the snow density with ρ_1 and ρ_2 representing the aggregates and graupel, respectively. Figure 11 shows the comparisons of the computational results of D_0 and N_T as the snow densities and μ are chosen at several values. Differences of the results between $\rho = (0.2, 0.8)$ (solid lines) and $\rho = (0.1, 0.6)$ (dashed lines) at $\mu = 2$ in Fig. 11 exhibit the dependence of the estimated D_0 and N_T on the snow density. As expected, the D_0 has little change with change of snow densities. In contrast, the N_T changes dramatically. In view of the comparisons between $\mu = 0$ (dotted-dashed lines) and $\mu = 2$ for the snow densities $\rho = (0.2, 0.8)$, a change of μ alters the results of both D_0 and N_T but in different degrees. The consistency of the radar-derived size distributions has been checked by applying the dual-wavelength algorithm to the entire snow region of the T-39 radar measurements shown in Fig. 6a. Illustrated in Fig. 12 are the results of the retrieved D_0 and N_T for snow in the region above 5 km. In the retrieval, the snow is classified as aggregates in the area where the DFR is greater than 3 dB and as graupel in the area where the DFR is less than 3 dB as

determined from the data shown in Fig. 6b. As in Figs. 6c and 6d, the snow densities of aggregates and graupel are assumed to be 0.2 and 0.7 g cm^{-3} , respectively. Although the only in situ data available were from the

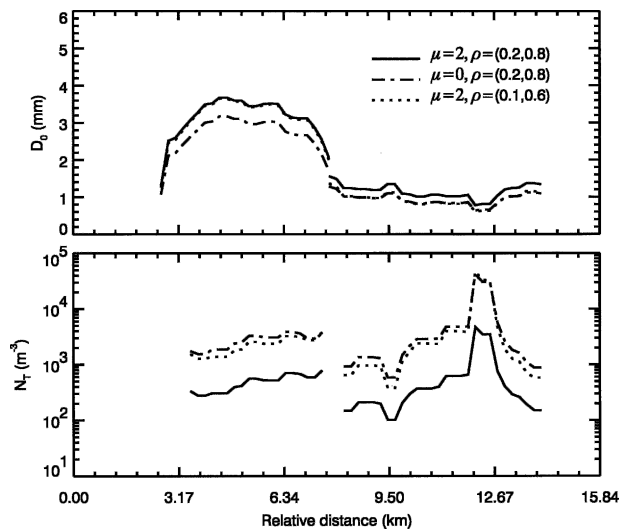


FIG. 11. Comparisons of (top) D_0 and (bottom) N_T retrieved from the data of the T-39 radar shown in Figs. 6a,b at the different μ and the combinations of the snow densities. For example, the combination of the snow densities, $\rho = (0.1, 0.6)$, stands for the snow densities of 0.1 g cm^{-3} for aggregates and 0.6 g cm^{-3} for graupel, respectively.

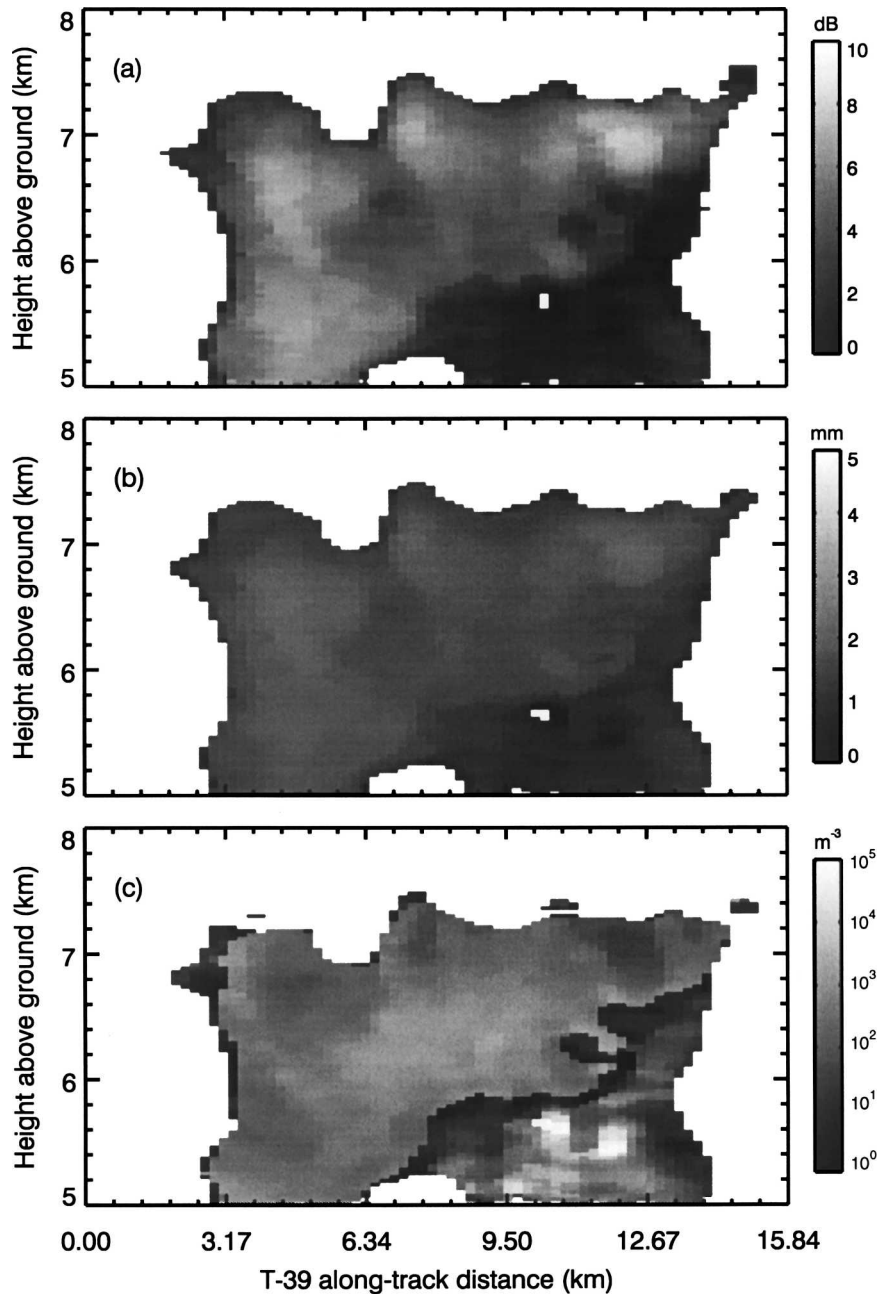


FIG. 12. Maps of D_0 and N_T derived from the T-39 radar measurements, as shown in Fig. 6a, within the snow region where the altitude of radar echoes is greater than 5 km above the surface: (a) measured DFR of X and Ka bands, (b) D_0 in mm, and (c) N_T in m^{-3} .

T-28 flight lines at 5.2 km, the results for D_0 and N_T in Figs. 12b and 12c appear to be reasonably consistent with the in situ data.

We conclude that the median volume diameter of snow can be estimated reasonably well from dual-wavelength airborne radar operating at X and Ka bands. On the other hand, N_T is affected by the assumptions of the snow density and the shape factor of the

gamma distribution and can be accurately estimated only if the snow density and μ are known. The empirical relations that connect the snow density to the snow size, such as those given by Magono and Nakamura (1965) and Klaassen (1988), along with the information on μ based on a statistical analysis of in situ particle measurements may improve the accuracy for the snow parameter retrievals.

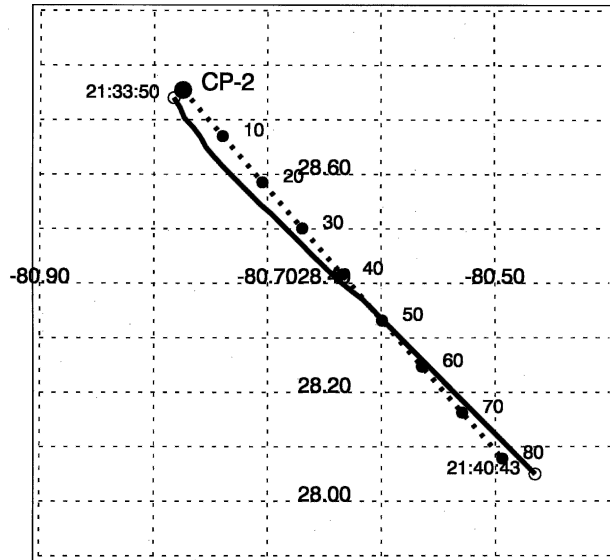


FIG. 13. Map of the T-39 flight track (solid line) in reference to the NCAR CP-2 radar. The dashed line represents direction along which the RHI scan of the CP-2 was taken. Distances in km from the CP-2 are shown along the dashed line.

4. Comparison with ground-based radar

During CaPE the T-39 was also coordinated with measurements from the ground-based NCAR CP-2 radar that operated at S and X bands. With the measurements of the CP-2 radar at two wavelengths the D_0 , as shown in Figs. 3 and 4, can be estimated by the same procedure used for the X- and Ka-band data. As such, the consistency of the dual-wavelength radar algorithm can be further examined by comparing estimated parameters of the particle size distributions from the collocated measurements between the ground and airborne radars. A challenge for this work is to precisely register the datasets, taken from two platforms, into the same coordinates. To map the data we first project the T-39 data onto the horizontal direction along which the RHI scan of the CP-2 radar was made. By applying a cross-correlation of the T-39 and CP-2 radar data, the registration of the datasets proceeds by shifting the T-39 radar measurements along the horizontal direction of the CP-2 until the cross-correlation is maximized.

Shown in Fig. 13 is a set of observations of the T-39 and CP-2 radars taken on 16 July 1991 over a stratiform portion of a storm. The T-39 flight track (solid line) for the time period 2133:50–2140:43 UTC is approximately collocated with the RHI scan (dashed line) of the CP-2 radar at 2137:28 UTC. Over a nearly 75-km flight leg over the rain, the spatial offsets between the T-39 and CP-2 were smaller than 5 km for ranges, as measured

from the CP-2, of less than 40 km. For ranges beyond 40 km the T-39 was nearly perfectly aligned along the CP-2 radial direction. The measured reflectivities of the airborne and ground-based radars are remapped in Fig. 14 as a function of radial distance from the CP-2 radar by means of the registration procedure described earlier. As shown in Fig. 14, the two radars exhibit very similar storm structures except for a gap (missing data) in the T-39 radar data. With its fairly high vertical resolution (30 m) the bright band is well defined by the T-39 airborne radar. For the case of the CP-2 radar, where the vertical resolution degrades gradually as the horizontal range increases, the bright band is clearly detected only for distances less than about 40 km. Unlike the T-39 X- and Ka-band radar, the DFR for S and X bands are relatively small and the estimates appear noisy. Thus, an estimate of D_0 from the S and X bands requires averaging a sufficiently large number of measurements in time and space so that the DFR can be effectively extracted. For this reason, the comparisons of the snow parameters between the CP-2 and T-39 radars are restricted to the mean vertical and horizontal profiles of DFR.

To compare the T-39 and CP-2 radar estimates, the data are used only if the reflectivity factors measured from each radar exceeds its respective minimum detectable signal. Plotted in Fig. 15 are the vertical (top) and horizontal (bottom) profiles of the D_0 estimated from the mean profiles of DFR in the snow region (above radar bright band). Because of appearance of the radar bright band as shown in Fig. 14, the measurements are associated with stratiform storm in which the aggregates typically dominate. The snow density is therefore taken to be 0.2 g cm^{-3} and μ to be -0.5 for the radar retrieval of D_0 , which is consistent with the values used in Fig. 6 for the case of aggregates. Although the D_0 from the CP-2 data, as expected, exhibits large fluctuations, it nevertheless shows clear trends in both vertical and horizontal directions. In general, these trends are consistent with the more stable results from the T-39 radar data. Overall, the estimates of D_0 of the T-39 and CP-2 radar data are correlated fairly well for both the vertical and horizontal profiles. It is worth mentioning that the profiles of D_0 from the CP-2 radar are sensitive to the assumed values of snow density and μ used in the retrieval while those from the T-39 radar remain relatively stable, independent of the snow density and μ . This difference can be understood by comparing the results of Figs. 1 and 2 with those of Figs. 3 and 4; in particular, the fractional error in D_0 with changes in ρ and μ is much smaller for the 10- and 35-GHz combination than it is for the 3- and 10-GHz set. Note that the reflectivities of the S and X bands of the CP-2 radar,

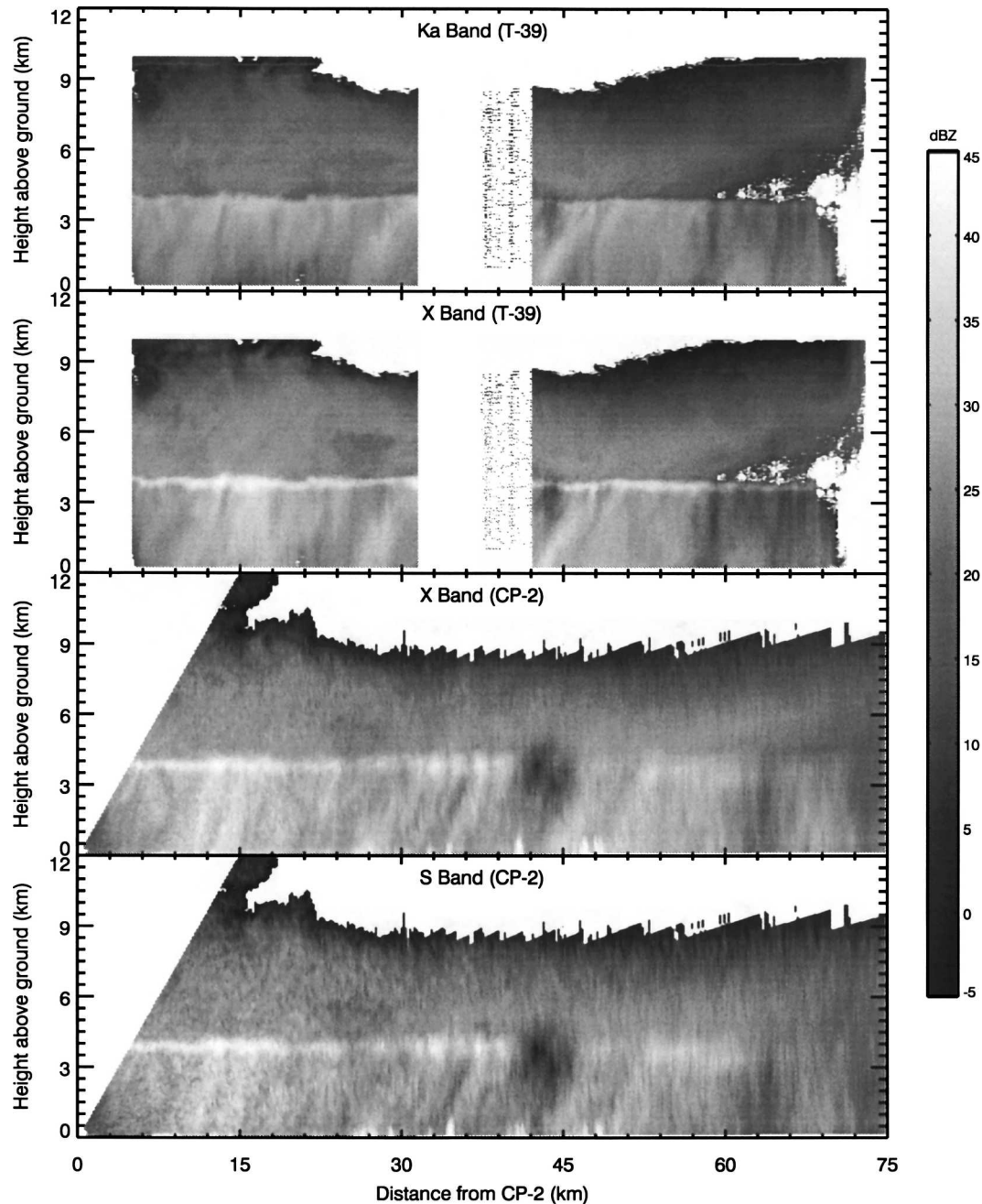


FIG. 14. Radar-measured reflectivity factors of the (top two images) T-39 airborne radar and the (bottom two images) CP-2 ground radar in terms of the distance from the CP-2. The data are the measurements corresponding to the T-39 flight track and the CP-2 RHI scan, shown as the solid and dashed lines in Fig. 13, respectively.

used for the estimates of the snow parameters, have been corrected to take into account the rain attenuation by using standard $K-Z$ relations (Battan 1973), where k is the specific attenuation coefficient (dB km^{-1}). The results of N_T from the CP-2 radar (not shown) fluctuate strongly because of the dependence on the snow density and μ . As a result of this uncertainty, the comparisons of N_T are not instructive.

5. Summary

A description was presented of a dual-wavelength radar algorithm to estimate characteristics of the snow size distribution. For the cases of the airborne T-39 and ground-based CP-2 radars, the computations of the DFR, with respect to the several snow densities and μ , were made as a function of D_0 . Analysis of the results

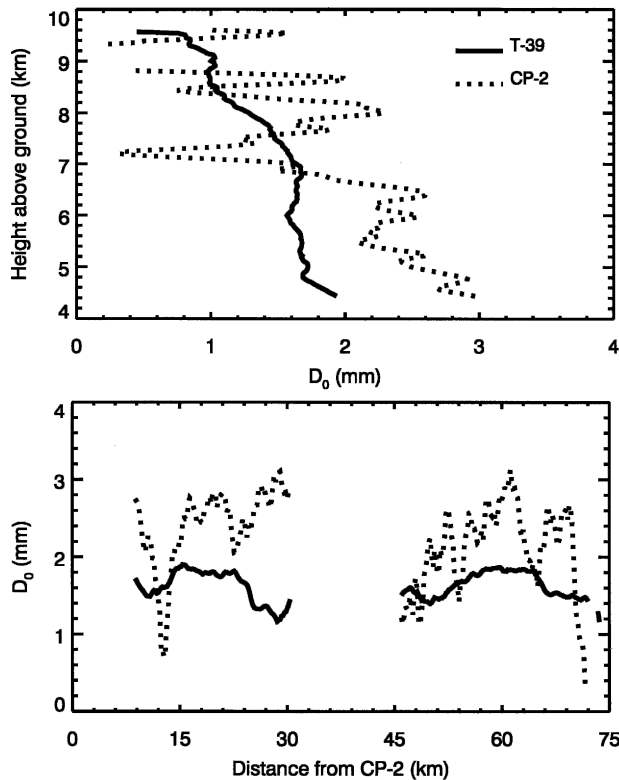


FIG. 15. Comparisons of the (top) vertical and (bottom) horizontal profiles of D_0 as derived from the T-39 airborne and CP-2 ground-based radars in the snow region.

indicates that the DFR– D_0 relations for the pair of the X- and Ka-band wavelengths of the T-39 radar are nearly independent of the snow density for most values of D_0 , and have only modest sensitivity to the μ parameter of the gamma size distribution. The fact that the DFR depends primarily on D_0 suggests that accurate estimates of the particle size distributions should be possible if the particles are sufficiently large relative to the shorter wavelength and if the attenuation can be either neglected or corrected. Once D_0 is estimated, the N_T can be directly derived from either of the reflectivities at two wavelengths. The N_T , however, depends on the snow density and the assumed μ . This may lead to an error if an inaccurate snow density or μ are used. The results also indicate that the combination of X and Ka bands is far superior in terms of stability and accuracy to the S- and X-band combination for inferring snow characteristics as long as attenuation from cloud water can either be neglected or corrected.

Validation of the dual-wavelength techniques was performed by comparing the derived snow parameters and size distributions from the T-39 airborne radar with direct particle measurements. Having carefully regis-

tered the particle information obtained from the aircraft in situ PMS measurements, the radar-derived characteristic snow parameters and size distributions were compared with the measurements. We find that the radar results agree reasonably well with those from the direct measurements by the PMS. Moreover, based on an examination of the PMS 2D images, the signatures of the DFR of the T-39 radar are quite sensitive to the type of the snow particle. From the measurements of the T-39 radar used in our study, the DFR of aggregates appears to be several times greater than that for the graupel. This feature of the DFR, if true for general cases, should help to identify snow type by means of the dual-wavelength radar. Confirmation of this feature requires further study as well as more coordinated radar and particle in situ measurements. It is also found, from the comparisons, that use of the snow densities of 0.2 g cm^{-3} for aggregates and 0.7 g cm^{-3} for graupel for the radar retrieval gives the best agreement. The shape factors of the gamma size distributions are -0.5 for aggregates and 1 for graupel based on the parametric fits of the in situ particle measurements.

To check the consistency of the retrieval, comparisons of D_0 estimates were also made using the T-39 airborne and ground-based CP-2 radars for a stratiform storm from one set of coordinated measurements. Due to the strong fluctuations of the DFR from the CP-2 radar, the comparisons are made only on the mean profiles of the horizontal and vertical measurements of snow above the radar bright band. With the use of the snow density of 0.2 g cm^{-3} and μ of -0.5 , it is shown that the retrievals of D_0 from both radars are consistent despite the fluctuations of the results from the CP-2. We conclude that the use of dual-wavelength radar, with properly chosen wavelengths, should provide useful estimates of the microphysical properties of hydrometeors. The GPM precipitation radar, operating at frequencies of Ku band (13.8 GHz) and Ka band, has a great deal of similarity to the X- and Ka-band combination used on the aboard T-39 aircraft in terms of the general behavior of the DFR– D_0 relationship. As a consequence, our findings in this study have direct applications to estimation of snow in mid and high-latitude regions. It is anticipated that the GPM radar will play an important role in mapping the microphysical properties of hydrometeors globally.

Acknowledgments. We wish to thank NCAR for providing the CP-2 radar data and its processing software. The T-28 operations were supported by the NSF Lower Atmospheric Observing Facilities program. We wish to thank Peter Bradfield and GSFC/Wallops Flight Facility for support of the T-39 operations.

REFERENCES

- Battan, L. J., 1973: *Radar Observation of the Atmosphere*. University of Chicago, 324 pp.
- Boucher, R. J., and J. G. Wieler, 1985: Radar determination of snowfall rate and accumulation. *J. Climate Appl. Meteor.*, **24**, 68–73.
- Braham, R. R., Jr., 1990: Snow particle size spectra in lake effect snows. *J. Appl. Meteor.*, **29**, 200–207.
- Bringi, V., G. Huang, V. Chandrasekar, and E. Gorgucci, 2002: A methodology for estimating the parameters of a gamma rain-drop size distribution model from polarimetric radar data: Application to a squall-line event from the TRMM/Brazil campaign. *J. Atmos. Oceanic Technol.*, **19**, 633–645.
- Bruggeman, D. A. G., 1935: Berechnung verschiedener Konstanten von heterogenen Substanzen: I. Dielectricitätskonstanten und Leitfähigkeiten der Mischkörper aus isotropen Substanzen. *Ann. Phys.*, **24**, 636–679.
- Carlson, R. E., and J. S. Marshall, 1972: Measurement of snowfall by radar. *J. Appl. Meteor.*, **11**, 494–500.
- Debye, P., 1929: *Polar Molecules*. Dover, 172 pp.
- Gorgucci, E., G. Scarchilli, V. Chandrasekar, and V. Bringi, 2000: Measurement of mean raindrop shape from polarimetric radar observations. *J. Atmos. Sci.*, **57**, 3406–3413.
- , —, —, and —, 2002: Estimation of raindrop size distribution parameters from polarimetric radar measurements. *J. Atmos. Sci.*, **59**, 2373–2384.
- Gunn, K. L. S., and J. S. Marshall, 1958: The distribution with size of aggregate snowflakes. *J. Meteor.*, **15**, 452–461.
- Iguchi, T., R. Oki, E. A. Smith, and Y. Furuhashi, 2002: Global Precipitation Measurement program and the development of dual-frequency precipitation radar. *J. Commun. Res. Lab.*, **49**, 37–45.
- Imai, I., M. Fujiwara, I. Chimura, and Y. Toyama, 1955: Radar reflectivity of falling snow. *Pap. Meteor. Geophys.*, **6**, 130–139.
- Klaassen, W., 1988: Radar observations and simulation of the melting layer of precipitation. *J. Atmos. Sci.*, **45**, 3741–3753.
- Liao, L., and R. Meneghini, 2000: Investigation of the dielectric constants of inhomogeneous air-ice and snow-water spheres. *Proc. IEEE 2000 Int. Geoscience and Remote Sensing Symp.*, Honolulu, HI, IEEE, 1804–1806.
- , —, T. Iguchi, and A. Detwiler, 1997: Estimation of snow parameters from dual-wavelength airborne radar. Preprints, *28th Conf. on Radar Meteorology*, Austin, TX, Amer. Meteor. Soc., 510–511.
- Löffler-Mang, M., and U. Blahak, 2001: Estimation of the equivalent radar reflectivity factor from measured snow size spectra. *J. Appl. Meteor.*, **40**, 843–849.
- Magono, C., 1957: On snowflakes. *Proc. Sixth Weather Radar Conf.*, Cambridge, MA, Amer. Meteor. Soc., 31–36.
- , and T. Nakamura, 1965: Aerodynamic studies of falling snow flakes. *J. Meteor. Soc. Japan*, **43**, 139–147.
- Mardiana, R., T. Iguchi, and N. Takahashi, 2004: A dual-frequency rain profiling method without the use of surface reference technique. *IEEE Trans. Geosci. Remote Sens.*, **42**, 2214–2225.
- Matrosov, S. Y., 1992: Radar reflectivity in snowfall. *IEEE Trans. Geosci. Remote Sens.*, **30**, 454–461.
- , 1998: A dual-wavelength radar method to measure snowfall rate. *J. Appl. Meteor.*, **7**, 1510–1521.
- Maxwell-Garnett, J. C., 1904: Colors in metal glasses and in metallic films. *Philos. Trans. Roy. Soc. London*, **203A**, 385–420.
- Meneghini, R., and H. Kumagai, 1994: Characteristics of the vertical profiles of dual-frequency, dual-polarization radar data in stratiform rain. *J. Atmos. Oceanic Technol.*, **11**, 701–711.
- , and L. Liao, 1996: Comparisons of cross sections for melting hydrometeors as derived from dielectric mixing formulas and a numerical method. *J. Appl. Meteor.*, **35**, 1658–1670.
- , and —, 2000: Effective dielectric constants of mixed-phased hydrometeors. *J. Atmos. Oceanic Technol.*, **17**, 628–640.
- , T. Kozu, H. Kumagai, and W. C. Bonczyk, 1992: A study of rain estimation methods from space using dual-wavelength radar measurements at near-nadir incidence over ocean. *J. Atmos. Oceanic Technol.*, **9**, 364–382.
- , H. Kumagai, J. Wang, T. Iguchi, and T. Kozu, 1997: Microphysical retrievals over stratiform rain using measurements from an airborne dual-wavelength radar-radiometer. *IEEE Trans. Geosci. Remote Sens.*, **29**, 690–703.
- Ohtake, T., 1968: Change of size distribution of hydrometeors through a melting layer. *Proc. 13th Radar Meteorology Conf.*, Montreal, QC, Canada, Amer. Meteor. Soc., 148–153.
- Sekhon, R. S., and R. C. Srivastava, 1970: Snow size spectra and radar reflectivity. *J. Atmos. Sci.*, **27**, 299–307.
- Simpson, J., C. Kummerow, W.-K. Tao, and R. F. Adler, 1996: On the Tropical Rainfall Measuring Mission (TRMM). *Meteor. Atmos. Phys.*, **60**, 19–36.
- Smith, P. L., 1984: Equivalent radar reflectivity factors for snow and ice particles. *J. Climate Appl. Meteor.*, **23**, 1258–1260.
- Vivekanandan, J., G. Zhang, and M. K. Politovich, 2001: An assessment of droplet size and liquid water content derived from dual-wavelength radar measurements to the application of aircraft icing detection. *J. Atmos. Oceanic Technol.*, **18**, 1787–1798.